CHEMISTRY OF MATERIALS

Article

pubs.acs.org/cm

Hydrogen Storage in the Expanded Pore Metal–Organic Frameworks M_2(dobpdc) (M = Mg, Mn, Fe, Co, Ni, Zn)

David Gygi,[†] Eric D. Bloch,[†] Jarad A. Mason,[†] Matthew R. Hudson,[‡] Miguel I. Gonzalez,[†] Rebecca L. Siegelman,[†] Tamim A. Darwish,[⊥] Wendy L. Queen,[§,#] Craig M. Brown,[‡,∥] and Jeffrey R. Long*[,†,▽]

[†]Department of Chemistry, University of California, Berkeley and Materials Sciences Division, Lawrence Berkeley National Laboratory, Berkeley, California 94720, United States

[‡]Center of Neutron Research, National Institute of Standards and Technology, Gaithersburg, Massachusetts 20899, United States

[§]The Molecular Foundry, Lawrence Berkeley National Laboratory, Berkeley, California 94720, United States

[∥]Chemical and Biomolecular Engineering, University of Delaware, Newark, Delaware 19716, United States

[⊥]National Deuteration Facility, Australian Nuclear Science and Technology Organisation, Lucas Heights, Australia

[#]Department Institut des Sciences et Ingénierie Chimiques, Ecole Polytechnique Fédérale de Lausanne—Valais Wallis (EPFL), CH 1951 Sion, Switzerland

[▽]Department of Chemical and Biomolecular Engineering, University of California, Berkeley, California 94720, United States

Supporting Information

ABSTRACT: The hydrogen storage properties of a new family of isostructural metal–organic frameworks are reported. The frameworks M_2(dobpdc) (M = Mg, Mn, Fe, Co, Ni, Zn; dobpdc^{4-} = 4,4′-dioxidobiphenyl-3,3′-dicarboxylate) are analogous to the widely studied M_2(dobdc) (M = Mg, Mn, Fe, Co, Ni, Cu, Zn; dobdc^{4-} = 2,5-dioxido-1,4-benzenedicarboxylate) family of materials, featuring the same weak-field oxo-based ligand environment for the M^{2+} metal centers, but with a larger pore volume resulting from the extended length of the dobpdc^{4-} linker. Hydrogen gas adsorption isotherms measured at 77 and 87 K indicate strong H_2 binding at low pressures, corresponding to the adsorption of one molecule per M^{2+} site. Isosteric heats of adsorption indicate adsorption enthalpies ranging from −8.8 to −12.0 kJ/mol, with the trend Zn < Mn < Fe < Mg < Co < Ni. Room-temperature high-pressure adsorption isotherms indicate enhanced gravimetric uptakes compared to the M_2(dobdc) analogues, a result of the higher surface areas and pore volumes of the expanded frameworks. Indeed, powder neutron diffraction experiments performed on Fe_2(dobpdc) reveal two additional secondary H_2 adsorption sites not observed for the nonexpanded framework. While displaying higher gravimetric capacities than their nonexpanded counterparts, the larger pore volumes result in lower volumetric capacities. Upon comparison with other promising frameworks for hydrogen storage, it becomes evident that in order to design future materials for on-board hydrogen storage, care must be placed in achieving both a high surface area and a high volumetric density of exposed metal cation sites in order to maximize gravimetric and volumetric capacities simultaneously.

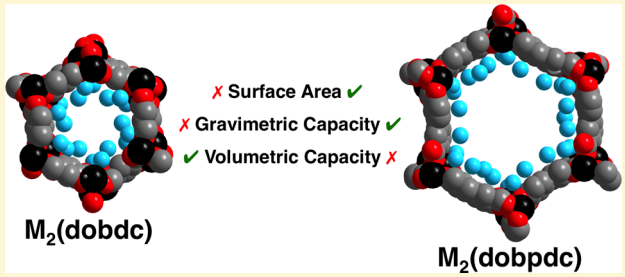

INTRODUCTION

As a potentially renewable and gravimetrically dense fuel, hydrogen stands poised as a clean burning alternative to current carbon based fuels.[1−3] However, limited on-board storage capacity remains a major obstacle to its widespread implementation, preventing it from being competitive with gasoline. In order to achieve a target driving range of 300 miles for fuel-cell-based light-duty vehicles, the Department of Energy has identified specific targets for hydrogen storage systems. Targets of a 5.5 wt % H_2 gravimetric capacity and a volumetric capacity of 40 g of H_2/L are based on the mass and volume of the entire system and must be achievable from −40 to 60 °C with a maximum pressure of 100 bar. Refueling rate, durability, and cost are also important considerations.[4] A number of competing technologies are currently under investigation for onboard hydrogen storage, including metal hydrides,[5] cryogenic storage,[6] and ultra high-pressure storage.[7] Although metal hydrides exhibit high volumetric storage capacities, they suffer gravimetrically and can involve expensive metals. Cryogenic storage requires a heavy, voluminous, and expensive on-board system in order to maintain the requisite low temperatures. High-pressure storage in cylinders typically requires pressures of 700 bar for appreciable driving distances,

Received: November 24, 2015
Revised: January 23, 2016
Published: January 28, 2016

DOI: 10.1021/acs.chemmater.5b04538
Chem. Mater. 2016, 28, 1128−1138

which entails the use of expensive compressors and heavy, bulky fuel tanks.[7]

Recently, adsorptive storage employing porous materials has been explored as a possible alternative to current hydrogen storage technologies. Although activated carbons and zeolites have been widely studied and are typically cheap, abundant, and nontoxic materials, they do not meet the gravimetric and volumetric storage targets because of their relatively weak interactions with H_2.[8,9] Indeed, the adsorption enthalpies within these materials are significantly lower than the −15 to −20 kJ/mol needed to achieve a reasonable storage capacity at ambient temperature and 100 bar.[10,11] Metal−organic frameworks represent a promising, relatively new, and tunable class of materials that may have the potential to meet the aforementioned storage targets.[12−22]

MOF-5 ($Zn_4O(bdc)_3$; bdc^{2-} = 1,4-benzenedicarboxylate), a high surface area material that has been among the most widely studied metal−organic frameworks, boasts an exceptional gravimetric uptake of 10 wt % and a volumetric storage density of 66 g H_2/L at 100 bar and 77 K.[17] The latter value represents a significant improvement over the density of pure hydrogen under these conditions (31 g/L at 77 K and 100 bar). However, at 298 K the adsorption capacity of this material decreases dramatically to 8.9 g/L, which represents little improvement over the density of pure hydrogen at the same temperature and pressure (8.7 g/L). The relatively poor performance of this material at room temperature is a result of the weak interaction between H_2 and the framework surface, which at −5.0 to −6.9 kJ/mol, falls short of the target enthalpy necessary for optimal storage and delivery.[10,11] A number of high surface area metal−organic frameworks with the potential to improve upon the gravimetric storage capacity of MOF-5 have since been synthesized.[23−25] In order to access expanded framework topologies, acetylene and phenyl spacers have been added to previously used linkers. These expanded materials can display BET surface areas in excess of 7000 m^2/g and exceptional gravimetric storage capacities at cryogenic temperatures; however, they exhibit adsorption capacities of just ∼1 wt % at 298 K and 100 bar and comparably low volumetric uptakes, in part due to their lack of strong binding sites.[26,27] Metal−organic frameworks containing stronger H_2 binding sites, such as materials featuring coordinatively unsaturated metal centers, often display higher room temperature capacities.

The $M_3[(M_4Cl)_3(BTT)_8]_2$ (M-BTT; BTT^{3-} = 1,3,5-benzenetristetrazolate; M = Mn, Fe, Co, Cu, Cd) family of frameworks was among the first metal−organic frameworks containing open metal sites studied for hydrogen storage.[28−32] This class of materials showed moderate improvements in volumetric capacity over materials lacking strong binding sites. In particular, Mn-BTT was the long-standing record holder for volumetric hydrogen storage, with a capacity of 12 g/L at 298 K and 90 bar.[28] This material, however, was unstable to complete desolvation, and as a result, its optimal potential as a hydrogen storage material was not achieved. In terms of hydrogen binding enthalpy, a moderate improvement over this material was realized with Fe-BTT, which displayed a low coverage isosteric heat of adsorption of −11.9 kJ/mol, but a 298 K and 100 bar capacity of just 8.4 g/L.[33]

Perhaps most representative of metal−organic frameworks containing accessible coordinatively unsaturated metal sites is the well-known $M_2(dobdc)$ ($dobdc^{4-}$ = 2,5−dioxido−1,4−benzenedicarboxylate; M-MOF-74; CPO-27-M) framework family. Thus, far, eight different isostructural analogues with M = Mg, Mn, Fe, Co, Ni, Cu, Zn, and Cd have been synthesized.[34−41] Comparable libraries of accessible metal cations within an isostructural series of frameworks are found only in the $M_3(btc)_2$ (btc^{3-} = 1,3,5-benzenetricarboxylate; M = Cr, Fe, Ni, Co, Cu, Zn, Mo, Ru), M-BTT (M = Mn, Fe, Co, Cu, Cd), and M-MOF-5 (M = Ti, V, Cr, Mn, Fe, Co, Ni) frameworks.[28−32,42−46] These $M_2(dobdc)$ frameworks have been widely studied for a variety of applications, including conductivity,[47−50] drug delivery,[51,52] catalysis,[53−55] and the storage and separation of various gases.[56−68] Intense scrutiny has been placed on this particular class of materials as a result of their high gravimetric and volumetric density of open metal sites and relatively high thermal and hydrolytic stability. Furthermore, the compatibility of this structure type with the incorporation of a wide array of metal ions allows for the systematic study of fundamental metal−adsorbate interactions.[69−72]

Isosteric heats of hydrogen adsorption in $M_2(dobdc)$ suggest the population of a first strong binding site, followed by the occupation of additional binding sites with lower enthalpies of adsorption. This is further corroborated by the distinct change in adsorption isotherm shape upon reaching approximately one H_2 per metal site. Confirmation of the presence of a primary strong binding site and several additional weaker binding sites was realized through the use of neutron diffraction. Neutron diffraction studies undertaken with $M_2(dobdc)$ (M = Mg, Fe, Co, Ni, Zn) reveal M^{2+}−D_2 distances for the primary binding site of 2.20(1)−2.60 Å with Ni < Co < Mg < Fe < Zn.[70,73,74] Additionally, the M−D_2 bond distances correlate well with the adsorption enthalpies, with $Ni_2(dobdc)$ having the highest initial enthalpy of −12.9 kJ/mol and $Zn_2(dobdc)$ the lowest of −8.5 kJ/mol.[72−74] Additional weaker binding sites were identified in each case, accounting for the drop of the isosteric heat to a lower value after saturation of the strong binding sites at a loading of ∼1 H_2 per M.

Two different expanded analogues of $M_2(dobdc)$ have recently been synthesized. Although both are based on the dioxidobiphenyl-dicarboxylate ligand, the placement of the carboxylate and phenoxy units is switched in each isomer. The so-called IRMOF-74-II framework utilizes 3,3′-dioxidobiphenyl-4,4′-dicarboxylate and has been synthesized with Mg^{2+} and features one-dimensional hexagonal channels with ∼19 Å pores and a BET surface area of 2510 m^2/g.[75] Our laboratory concurrently developed the isomorphous framework series based upon 4,4′-dioxidobiphenyl-3,3′-dicarboxylate ($dobpdc^{4-}$). Thus far, six different $M_2(dobpdc)$ materials have been synthesized with M = Mg, Mn, Fe, Co, Ni, and Zn. A single crystal X-ray analysis of $Zn_2(dobpdc)$ enabled the first structural characterization of this material, while the magnesium analogue proved to be an exceptional scaffold for appending diamines, resulting in a material with high a CO_2 adsorption capacity and CO_2/N_2 selectivity for capture from both air and under flue gas conditions.[76,77] We recently extended this strategy to the remaining members of the $M_2(dopbdc)$ family to prepare a new class of "phase-change" adsorbents that display unusual step-shaped CO_2 isotherms that shift drastically with temperature.[78] This behavior is not seen in the nonexpanded $M_2(dobdc)$ frameworks.

Herein, as part of an ongoing effort to improve high pressure hydrogen storage in metal−organic frameworks with exposed metal sites, we investigate in detail the H_2 adsorption properties of the expanded isoreticular materials $M_2(dobpdc)$ (M = Mg, Mn, Fe, Co, Ni, Zn). The entire series is explored in order to

DOI: 10.1021/acs.chemmater.5b04538
Chem. Mater. 2016, 28, 1128−1138

study systematically the effects of both larger pores, possessing the potential for installation of additional binding sites, in addition to the variations in M−H_2 interactions.

EXPERIMENTAL PROCEDURES

General. Unless otherwise specified, all experimental procedures were conducted under an argon atmosphere using standard Schlenk techniques. All solvents, *N*,*N*′-dimethylformamide (DMF), methanol, 1,4-dioxane, and diethyl ether were obtained from commercial sources and used without further purification. All other reagents were obtained from commercial sources (Combi-Blocks and Sigma-Aldrich) at reagent grade purity or higher and used without further purification. NMR solvents were purchased from Cambridge Isotope Laboratories Inc. (MA, USA) and Sigma-Aldrich and were used without further purification. D_2O (99.8%) was supplied by Sigma-Aldrich. The M_2(dobpdc) (M = Mg, Mn, Fe, Co, Ni, Zn) frameworks were synthesized utilizing conditions recently reported by our laboratory.[78]

Instrumentation for Physical Measurements. Infrared spectra were collected on a PerkinElmer Spectrum 400 equipped with an attenuated total reflectance (ATR) accessory. Powder X-ray diffraction patterns were collected on a Bruker Advance D8 powder X-ray diffractometer employing Cu−Kα radiation (λ = 1.5418 Å) and equipped with a powder stage. Thermogravimetric analysis was carried out at a ramp rate of 2 °C/min in a nitrogen flow with a TA Instruments TGA 5000 apparatus. ^{1}H NMR spectra were obtained using a Bruker Avance 400 console with Oxford Instruments 9.39 T magnet.

Instrumentation for deuteration: Hydrothermal reactions were performed using a Mini Benchtop 4560 Parr Reactor (600 mL vessel capacity, 3000 psi maximum pressure, 350 °C maximum temperature). ^{1}H NMR (400 MHz), and ^{2}H NMR (61.4 MHz) spectra were recorded on a Bruker 400 MHz spectrometer at 298 K. Chemical shifts, in parts per million, were referenced to the residual signal of the corresponding NMR solvent. Deuterium NMR experiments were performed using the lock channel of the probe for direct observation. Electrospray ionization mass spectra (ESI-MS) were recorded on a 4000 QTrap AB Sciex spectrometer. The overall percentage deuteration of the molecules was calculated by NMR and MS using the isotope distribution analysis of the different isotopologues in MS.

*Synthesis of Methyl 5-Bromo-2-hydroxybenzoate (**1**).* A 500 mL round-bottom flask was charged with 5-bromosalicylic acid (10.0 g, 46.1 mmol), methanol (300 mL), and 98% sulfuric acid (10 mL). The reaction mixture was then heated at reflux (383 K) with stirring for 12 h and allowed to cool to room temperature, and the solvent was removed by rotary evaporation until approximately 50 mL of solvent remained and solid had precipitated. The white needle-like solid was collected by filtration and dried in air to yield 9.62 g (90%) of product. IR (ATR, neat): 3199 (m), 2961 (m), 1923 (w), 1773 (w), 1682 (vs), 1608 (s), 1598 (m), 1471 (s), 1435 (vs), (1336 (vs), 1285 (vs), 1242 (vs), 1198 (vs), 1102 (vs), 1078 (vs), 958 (vs), 828 (s), 787 (vs), 699 (vs), 626 (s) cm^{-1}. ^{1}H NMR (400 MHz, DMSO-d_6): 10.49 (s, 1H), 7.83 (d, J = 2.6 Hz, 1H), 7.64 (dd, J = 8.9, 2.6 Hz, 1H), 6.96 (d, J = 8.9 Hz, 1H), 3.87 (s, 3H).

*Synthesis of Methyl 2-Hydroxy-5-(4,4,5,5-tetramethyl-1,3,2-dioxaborola-yl)benzoate (**2**).* A 500 mL three-neck round-bottom flask was charged with **1** (8.00 g, 34.6 mmol), bis(pinacolato)diboron (8.79 g, 34.6 mmol), potassium acetate (10.2 g, 104 mmol), bis-(triphenylphosphine)-palladium dichloride (1.21 g, 1.73 mmol), and 1,4-dioxane (300 mL). The reaction mixture was then sparged with argon gas for 1 h, heated at reflux (383 K) with stirring for 24 h, and then cooled to ambient temperature under inert gas. The solution was filtered to remove palladium residue, and the filtrate was extracted with diethyl ether (3 × 150 mL). The organic extracts were combined, dried over anhydrous magnesium sulfate, and evaporated using a rotary evaporator to yield 6.25 g (65%) of an off-white crystalline powder. IR (ATR, neat): 2987 (m), 1673 (s), 1592 (s), 1441 (m), 1360 (s), 1307 (vs), 1286 (vs), 1273 (s), 1216 (vs), 1144 (vs), 1104 (vs), 1098 (s), 968 (s), 855 (s), 837 (s), 800 (vs), 754 (s), 694 (m), 659 (vs), 613 (m) cm^{-1}. ^{1}H NMR (400 MHz, DMSO-d_6): 10.80 (s, 1H), 8.11 (d, J = 1.6 Hz, 1H), 7.74 (dd, J = 8.3, 1.7 Hz, 1H), 6.97 (d, J = 8.3 Hz, 1H), 3.89 (s, 3H), 1.28 (s, 12H).

Synthesis of H_4(dobpdc). A 500 mL three-neck round-bottom flask was charged with **1** (5.00 g, 21.6 mmol), **2** (6.62 g, 23.8 mmol), potassium carbonate (6.58 g, 47.6 mmol), lithium chloride (101 mg, 2.38 mmol), 1,4-dioxane (150 mL), and water (150 mL) and sparged with argon for 1.5 h. Tetrakis(triphenylphosphine)palladium (826 mg, 0.714 mmol) was added to the reaction mixture under a counter-flow of argon, and the reaction was further heated at reflux (393 K) under an inert atmosphere for 27 h, cooled to ambient temperature, and then filtered to remove palladium residue. The filtrate was collected and acidified to pH 1 using 12 M HCl, causing a white precipitate to form. The precipitate was collected by filtration and dried in air to yield 4.20 g (71%) of a white powder. IR (ATR, neat): 3247 (m), 3073 (m), 2879 (m), 2634 (m), 2572 (m), 2130 (w), 1660 (vs), 1610 (vs), 1600 (s), 1479 (s), 1450 (vs), 1402 (m), 1310 (s), 1290 (vs), 1217 (vs), 1151 (m), 1100 (m), 1052 (m), 971 (w), 911 (m), 875 (m), 831 (s), 792 (s), 724 (w), 685 (s), 656 (s) cm^{-1}. ^{1}H NMR (400 MHz, DMSO-d_6): 14.12 (s, 1H), 11.31 (s, 1H), 7.96 (d, J = 2.5 Hz, 1H), 7.79 (dd, J = 8.6, 2.5 Hz, 1H), 7.04 (d, J = 8.6 Hz, 1H).

Synthesis of 4,4′-Biphenol-d_8. A mixture of 4,4′-biphenol (5.0 g, 27 mmol), Pt/activated carbon (1.0 g, 10 wt % of the substrate, 0.51 mmol Pt), and 40% w/w NaOD (6 g, 59 mmol) in D_2O (120 mL) was loaded into a Parr pressure reactor. The contents of the reactor were degassed by purging with N_2 gas, and the reactor was subsequently purged with an atmosphere of H_2 gas and then sealed and heated to 180 °C with constant stirring for 1 day. The reactor was cooled to room temperature, and the contents were filtered through a short plug of Celite to remove the catalyst, which was further washed with water (150 mL). The aqueous filtrate was acidified to pH = 2 using 1 M HCl to produce a white precipitate, which was collected by filtration and washed with cold water. The residual water in the material was removed using a rotatory evaporator. Thin layer chromatography was used (referenced with the protonated compound) to estimate the purity and to develop a purification protocol. ^{1}H NMR (400 MHz) and ^{2}H NMR (61.4 MHz) spectra were recorded on a Bruker 400 MHz spectrometer at 298 K. The off white solid was dissolved in a minimum amount of acetone and reprecipitated by adding hexane, and the solid was collected and dried to give pure 4,4′-biphenol-d_8 (4.5 g, 90% yield, ≥ 97% D by NMR and MS). ^{1}H NMR (acetone-d_6): δ_H 6.87 (s, residual 4 × Ph-H), 7.40 (s, residual 4 × Ph-H), 8.31 (s, 2 × OH). ^{2}H NMR (acetone-d_6): δ_D 6.92 (bs, 4 × Ph-D), 7.45 (bs, 4 × Ph-D), 8.29 (bs, residual 2 × OD). ^{13}C{^{1}H} NMR (100.6 MHz, $CDCl_3$): δ_C 115.1 (t, 4 × Ph-D), 126.8 (t, 4 × Ph-D), 132.1 (s, qC), 156.2 (s, qC). ^{13}C{^{1}H,^{2}H} NMR (100.6 MHz, $CDCl_3$, D1 = 20 s): δ_C 115.1 (s, 4 × Ph-D) 126.8 (s, 4 × Ph-D), 132.1 (s, qC), 156.2 (s, qC). ESI-MS m/z: 193 [M-H]$^-$ overall 97.4% D levels with isotopic distribution d8 79.3%, d7 20.7%. (Supporting Information, Figures S28−S29).

Low-Pressure Gas Adsorption Measurements. For each low-pressure (0−1.2 bar) gas adsorption measurement, 200−500 mg of M_2(dobpdc) was transferred into a preweighed glass sample tube under an atmosphere of nitrogen gas and capped with a Transeal. Samples were then manually transferred to a Micromeritics ASAP 2020 gas adsorption analyzer and heated at a rate of 0.1 K/min to 453 K while under a vacuum. A sample was considered activated when the outgas rate at 453 K was less than 1 μbar/min. The evacuated tube containing the activated sample was then transferred to a balance and weighed to determine the mass of the desolvated sample. The tube was then manually placed on the analysis port of the instrument, where the outgas rate was once again confirmed to be less than 1 μbar/min. The N_2 adsorption isotherms were measured at 77 K in a bath of liquid N_2, while the H_2 measurements were carried out at 77 K in liquid N_2 and at 87 K in liquid Ar.

High-Pressure Gas Adsorption Measurements. High-pressure adsorption isotherms in the range of 0−100 bar were measured on a HPVA-II-100 from Particulate Systems, a Micromeritics company. In a typical measurement, 0.3−0.7 g of activated sample was loaded into a tared 2 mL stainless steel sample holder inside a glovebox under a N_2 atmosphere. Prior to connecting the sample holder to the VCR fittings

DOI: 10.1021/acs.chemmater.5b04538
Chem. Mater. 2016, 28, 1128−1138

of the complete high-pressure assembly inside the glovebox, the sample holder was weighed to determine the sample mass.

The fully assembled sample holder was transferred to an ASAP 2020 low-pressure adsorption instrument, fitted with an isothermal jacket, and evacuated at the original activation temperature of the material for at least 1 h. Then, a 77 K N_2 adsorption isotherm was measured. This was used to verify that the sample mass was correct and that the sample was still of high quality by comparing the resulting Langmuir surface area to the expected value. Note that a specially designed OCR adapter was used to connect the stainless steel high-pressure adsorption cell directly to the ASAP 2020 analysis port, allowing the measurement of accurate low-pressure isotherms on the exact same samples used for high-pressure measurements in the same sample holders.

The sample holder was then transferred to the HPVA-II-100, connected to the analysis port of the instrument via an OCR fitting, and evacuated at room temperature for at least 1 h. The sample holder was placed inside an aluminum recirculating Dewar connected to a Julabo FP89-HL isothermal bath filled with Julabo Thermal C2 fluid, for which the temperature stability is ±0.02 °C. Note that while the majority of the sample holder is placed inside the temperature bath (analysis zone), there is still a significant volume that is exposed to the air (ambient zone) and is affected by fluctuations in the temperature of the room. A small upper volume of the sample holder above the analysis port is inside a temperature controlled heated enclosure, along with the gas dosing manifold (manifold zone). While this setup is typical of most volumetric adsorption instruments, it creates challenges in determining the amount of free space (or empty volume) of the sample holder that is in each temperature zone. Accurately determining these volumes is particularly important, because non-ideality corrections have a significant temperature dependence that can lead to large errors at higher pressures. Thus, it is necessary to determine the volumes of the ambient and analysis temperatures zones for an empty sample holder. Since the portion of the sample holder containing the sample is always fully immersed in the constant temperature bath and the bath is always placed at the exact same height on the sample holder, the ambient volume will always be constant, regardless of the amount of sample present. On the other hand, the analysis volume will depend on the amount of sample present, but this can be easily determined by subtracting the volume of the sample from the analysis volume of the empty sample holder.

Here, the sample volume is determined by subtracting the total free space of the filled sample holder from that of the empty sample holder. The total free spaces for the empty or filled sample holders were determined using ambient temperature He free space measurements, which were repeated 20 times and averaged. The analysis volumes of the empty sample holder were determined by performing He free space measurements at each potential analysis temperature and calculated using the ideal gas law with the measured total empty volume of the sample holder, the ambient temperature, the analysis temperature, the He dose pressure, the He equilibrium pressure, the known dosing manifold volume, and the dosing manifold temperature. It is worth noting that by using this technique, it is only necessary to measure the He free space at ambient temperature for a new sample, and it is not necessary to measure He free space at any of the other analysis temperatures. High-pressure isotherms (0−100 bar) were then measured at 77, 248, 273, and 298 K.

Powder Neutron Diffraction Measurements. Neutron diffraction experiments were carried out at the National Institute of Standards and Technology Center for Neutron Research (NCNR) with 0.64 g of Fe_2(dobpdc-d_6) powder, using the high-resolution neutron powder diffractometer, BT1. The activated sample was placed in a He purged glovebox and subsequently loaded into a vanadium sample can, which was sealed using an indium O-ring and which contained an outlet valve for gas loading. Diffraction data were collected using a Ge(311) monochromator with an in-pile 60′ collimator corresponding to a wavelength of 2.078 Å. Before data collection, the sample was loaded onto a bottom-loading closed cycle refrigerator, connected to a gas-manifold of known volume, and the residual He evacuated at room temperature via turbo-molecular pump. Initial data on the evacuated, bare sample were collected at 10 K. For comparisons of the deuterium (D_2) loadings and structural dependence, approximately 0.75, 1.5, 2.75, and 4.5 D_2 molecules per Fe (refined composition given in Tables S4−S8) were successively dosed to Fe_2(dobpdc-d_6) at 77 K, and data were collected at 10 K. The sample was slowly cooled from 77 to 10 K to ensure full equilibration and complete adsorption, as evidenced by a zero pressure reading on the barometer above the condensation point.

Neutron diffraction data were analyzed by the Rietveld method as implemented in EXPGUI/GSAS.[79,80] The starting model for the activated Fe_2(dobpdc-d_6) compound was taken from a structure previously obtained from synchrotron X-ray diffraction data collected on the bare material at 100 K.[76] Initial refinement of the Fe_2(dobpdc-d_6) structure included free atomic displacement parameters (ADPs) for all atoms as well as "independent" H and D atoms on identical symmetry sites for the three unique ligand hydrogen atoms (H/D3, H/D5, H/D6) at an occupancy of 85% D and 15% H with a constrained net occupancy of 1. Attempts to refine the structure led to (i) poor thermal behavior in carbon atoms C2 and C5, as was observed in the 100 K synchrotron single crystal structure, and (ii) the occupancy of D3 and D5 refining to 100% deuterated while H6 refined to 100% hydrogenated, suggesting the total deuteration of Fe_2(dobpdc-d_6) at 67%. For the final refinement of the bare Fe_2(dobpdc-d_6) structure, ADPs for the carbon atoms were constrained to be identical based on the poor behavior of C2 and C5. Correspondingly, the ligand positional parameters (C1−C7, D3, D5, H6) were left in the ideal geometry from the single crystal refinement, as the behavior of the ligand in free refinement was less than ideal and the change in positional parameters for the ligand had no distinguishable impact on the refinement based on difference plot. Finally, the iron and coordinated oxygen atoms were left free to refine. ADPs for the oxygen atoms were constrained to be identical, as the refinement of these values led to the same results within a standard deviation. Note that D3, D5, and H6 were fixed at 100% D or H, respectively, for the subsequent deuterium dosed structure refinements, and the associated ADPs were constrained to be identical.

For the determination of D_2 adsorption sites in Fe_2(dobpdc-d_6), Fourier difference methods were employed to locate the adsorbed D_2 molecules. An initial dose of 0.75 D_2 per Fe was chosen to provide clarity in the structure model for the active site in eliminating potential D_2 intermolecular interactions, based upon previous knowledge of adsorption in the similar Fe_2(dobdc) material. Fourier mapping and accounting for a significant portion of the excess D_2 scattering density on the stable bare structural model, the atomic positions, and isotropic ADPs were left free to refine for both the iron centers and the added D_2 during the analysis. Upon determining that freeing the isotropic ADPs for the oxygen atoms, from one another, resulted in no appreciable difference in the model, these values were constrained to be equal and allowed to refine. Again, parameters for the positions were held at the values determined from the synchrotron single crystal experiments, as this did not affect the modeling of the D_2 within the confines of the framework, and the C ADPS were constrained to be identical to one another.

RESULTS AND DISCUSSION

Synthesis of M_2(dobpdc) (M = Mg, Mn, Fe, Co, Ni, Zn). The reaction of H_4(dobpdc) with divalent metal salts, under solvothermal conditions utilizing various alcohol/amide solvent mixtures, yielded highly crystalline microporous metal−organic frameworks that are isostructural with Zn_2(dobpdc), as determined by powder X-ray diffraction.[76] In order to achieve the isostrucutral series of frameworks, extensive screening of numerous reaction conditions with an array of alcohols (MeOH, EtOH, *i*-PrOH, *n*-BuOH), amides (DMF, DEF, DMA), and water was necessary. Small deviations in solvent mixtures or the use of older solvents yielded poorly crystalline and/or phase impure materials. Original screening procedures were performed on a 2 mL scale in 4 mL glass vials. Upon

DOI: 10.1021/acs.chemmater.5b04538
Chem. Mater. 2016, 28, 1128−1138

arriving at viable solvothermal conditions, all framework reactions were scaled up to a 10 mL scale in 20 mL glass scintillation vials. Attempts to further scale up reaction conditions to 100 mL and beyond were successful only for the Mg, Fe, and Ni frameworks. The remaining materials displayed decreases in crystallinity upon scaling up. Additionally, it was discovered that purging the reaction mixture with N_2 gas prior to heating yielded a more crystalline product and prevented formation of unwanted amorphous phases.

As noted above, the expanded frameworks display similar one-dimensional hexagonal channels to M_2(dobdc). The bridging ligands connect MO_6 units that form a three-dimensional structure with M^{2+} ions at the vertices of hexagons formed by connections via the organic linker. As is the case with M_2(dobdc), the as-synthesized expanded frameworks feature octahedral metal sites with a coordinated solvent molecule pointing into the channels. These solvent molecules can be removed by heating the materials under reduced pressure to create metal centers with square-pyramidal geometries and an open coordination site. The channels within M_2(dobpdc) have a larger diameter of 18−22 Å compared to those of the M_2(dobdc) compounds at 13−15 Å, depending on the metal cation. The larger pore diameter that results from the elongation of the ligand gives rise to a greater Langmuir surface area of 3000−3900 m^2/g for the M_2(dobpdc) compounds, compared to 1100−2100 m^2/g for the M_2(dobdc) compounds.[10,81]

The first coordination spheres of the metals in M_2(dobdc) and M_2(dobpdc) are nearly identical as a result of the similarities between H_4(dobdc) and H_4(dobpdc). As illustrated in Figure 1 for the single crystal structures of the cobalt analogs,

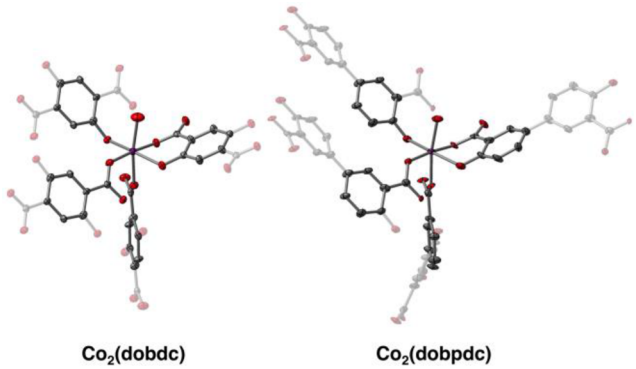

Figure 1. Coordination sphere for the cobalt cations in solvated Co_2(dobdc) (left) and Co_2(dobpdc) (right) as determined from single-crystal X-ray diffraction. Note the nearly identical cobalt−oxido and −carboxylato coordination. Purple, red, and gray spheres represent cobalt, oxygen, and carbon atoms, respectviely. Hydrogen atoms have been omitted.

the first coordination spheres of both M_2(dobdc) and M_2(dobpdc) feature two aryl oxide based oxygen ligands, while the remaining three are from carboxylates. The metal−oxygen bond distances are the same within error: the mean Co−O distance in Co_2(dobdc) is 2.08 ± 0.06 Å while in Co_2(dobpdc) it is 2.07 ± 0.05 Å. In addition, the Co−O bond distance with regard to the bound solvent molecule is 2.158(6) Å for Co_2(dobdc) (water molecule) and 2.114(1) Å for Co_2(dobpdc) (DEF molecule). As a result of the close similarities in the coordination environments for the open metal sites in these frameworks, they can be expected to display similar isosteric heats of H_2 adsorption when desolvated.

Low-Pressure H_2 Adsorption. In order to investigate the hydrogen storage properties of M_2(dobpdc), low pressure H_2 isotherms were measured at 77 and 87 K. The adsorption isotherms were independently fit with either a dual- or triple-site Langmuir model, as a single-site model did not yield an acceptable fit. This is consistent with a material that contains a mixture of high- and low-enthalpy H_2 binding sites. Using the dual- or triple-site Langmuir fits and the Clausius−Clapeyron equation, isosteric heats of adsorption, $-H_{ads}$, were calculated for each compound as a function of the amount of H_2 adsorbed. As shown in Figure 2A, all six frameworks display high initial

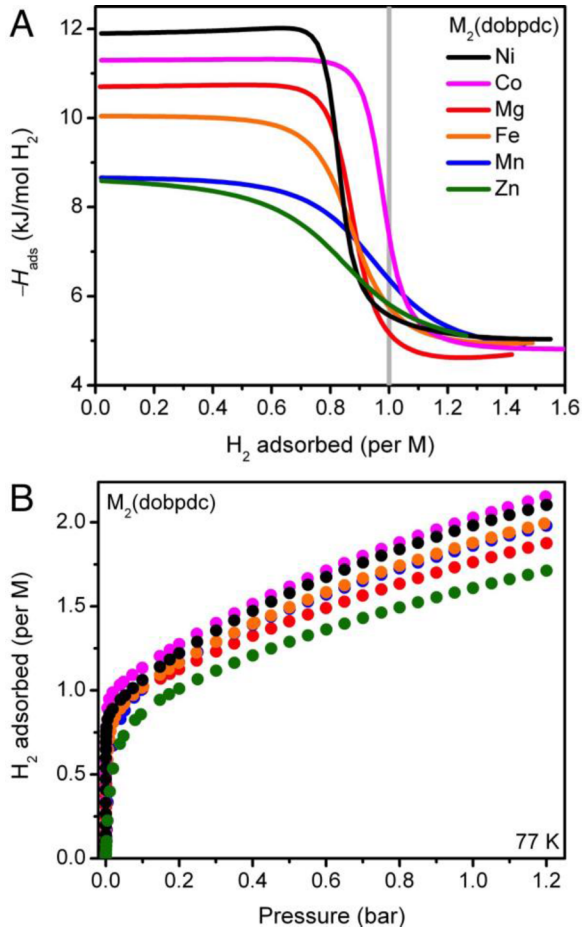

Figure 2. (A) Isosteric heats of adsorption plotted as a function of the amount of H_2 adsorbed for M_2(dobpdc). (B) Equilibrium H_2 adsorption isotherms for M_2(dobpdc) at 77 K. Note that the amount adsorbed is plotted in terms of H_2 molecules per M atom.

isosteric heats of adsorption that range from −8.4 to −12.0 kJ/mol with the magnitudes ordering as Ni > Co > Mg > Fe > Mn ~ Zn. The isosteric heats for all frameworks decrease rapidly to near −5 kJ/mol at higher loadings as the high-enthalpy metal sites become fully occupied.

The loading at which the isosteric heat decreases, or more specifically, the inflection point in the isosteric heat curve, can serve as a useful indicator of the completeness of framework activation and the accessibility of the open metal sites. If the inflection point resides at an H_2 loading of one molecule per open metal site, as is observed for Mn_2(dobpdc) and Co_2(dobpdc), then the framework is most likely completely

DOI: 10.1021/acs.chemmater.5b04538
Chem. Mater. 2016, 28, 1128−1138

desolvated and all open metal sites are accessible to H_2.[61] In contrast, if the inflection point in the isosteric heat curve occurs at a lower loading, as is observed for the other four compounds, then some fraction of the metal sites are not accessible to H_2. This could be the result of incomplete removal of bound solvent from some of the metal sites during activation or, more likely, from defects or intergrowth of crystallites that block some of the channels in the framework and make the metal sites inaccessible to gas molecules.[82−84]

Consistent with the M_2(dobdc) compounds, the trend in the low-coverage isosteric heats of adsorption across the M_2(dobpdc) family of frameworks tracks well with the empirical Irving−Williams series for high-spin octahedral divalent cations.[16,85] The zinc framework displays the lowest magnitude for the isosteric heat of adsorption at −8.4 kJ/mol, due to its $3d^{10}$ electron configuration. Otherwise, the magnitude of the isosteric heat tracks inversely with the ionic radius of the high-spin metal cation, with $Ni^{2+} > Co^{2+} > Fe^{2+} > Mn^{2+}$ (Table 1). Additionally, the magnesium framework exhibits an isosteric heat of adsorption comparable to that of Fe_2(dobpdc), due to the high charge density of the cation and the ionic nature of its interactions.

Table 1. Performance Metrics Comparison between the M_2(dobpdc) [M_2(dobdc)] Framework Families[34−41]

M	volumetric metal density (mmol M/cm^3)	gravimetric metal density (mmol M/g)	isosteric heat ($-Q_{st}$) (kJ/mol)	BET surface area (m^2/g)	Langmuir surface area (m^2/g)
Mg	3.54 [7.41]	6.28 [8.24]	10.7 [10.6]	3270 [1800]	3873 [2060]
Mn	3.53 [7.13]	5.28 [6.58]	8.7 [8.8]	2134 [1447]	3479 [1872]
Fe	3.53 [7.46]	5.23 [6.54]	10.0 [9.7]	2607 [1360]	3315 [1535]
Co	3.53 [7.49]	5.15 [6.41]	11.3 [10.7]	2255 [1341]	3357 [1432]
Ni	3.54 [7.74]	5.16 [6.42]	12.0 [12.9]	2059 [1218]	3108 [1312]
Zn	3.53 [7.57]	4.99 [6.15]	8.4 [8.5]	1873 [747]	2974 [1100]

Owing to the strong H_2 binding sites, the 77 K isotherms for all six frameworks (Figure 2B) display a sharp rise in H_2 uptake at low pressures (0−0.05 bar). In the case of cobalt and nickel, which exhibit the strongest hydrogen binding in the case of M_2(dobdc), a loading that corresponds to one H_2 molecule per metal site is achieved by just 10 mbar. The remaining four frameworks do not saturate their strongest binding sites until higher pressures, above 100 mbar in the case of Zn_2(dobpdc). The materials display a nearly linear increase in adsorption capacity up to 1.2 bar, ranging from 1.70 H_2 per metal for zinc to 2.15 H_2 per metal for cobalt with Zn < Mg < Mn ∼ Fe < Ni < Co. To illustrate the differences in low pressure H_2 adsorption between M_2(dobdc) and M_2(dobpdc), the 77 K adsorption isotherms for the nickel analogues are shown in Figure S22. On both a per metal and per gram basis, Ni_2(dobdc) displays a greater H_2 uptake capacity at pressures up to approximately 300 mbar as the nonexpanded framework contains a higher gravimetric density of open metal sites (6.42 vs 5.16 mmol/g) and has a slightly higher low-coverage isosteric heat. Given the much higher specific surface areas of M_2(dobpdc), on a gravimetric basis, these compounds can be expected to adsorb more hydrogen than M_2(dobdc) at higher pressures and therefore may show utility for H_2 storage at higher pressures.

Neutron Diffraction. Although single crystal X-ray diffraction has been utilized to structurally characterize metal−organic frameworks containing metal-bound molecules, it is often poorly suited for observing H_2 binding, due to the low X-ray scattering factor of a H atom.[86] We have previously shown neutron powder diffraction to be an invaluable technique for this challenging task.[39,52,62] Indeed, the structural characterization of a number of new species, including high-spin metal-paraffin, -olefin, -carbonyl, -CO_2, and -D_2 complexes, has been achieved in this manner. A particular obstacle to the utilization of neutron diffraction techniques for the M_2(dobpdc) family of frameworks is the higher density of hydrogen atoms on the ligand compared to the nonexpanded variant. In our hands, the high incoherent scattering of hydrogen in the extended dobpdc-based materials led to high background in neutron diffraction experiments, making analysis of weak high-angle diffraction peaks difficult. To combat this, we prepared a deuterated form of the ligand (H_4dobpdc-d_6) using previously reported methods and utilized it to synthesize Fe_2(dobpdc-d_6).[76]

A detailed powder neutron diffraction experiment was performed with Fe_2(dobpdc-d_6), allowing us to probe the exact positions, occupancies, and site affinities of adsorbed D_2 molecules (Figure 3). At a relatively low loading of 0.75 equiv

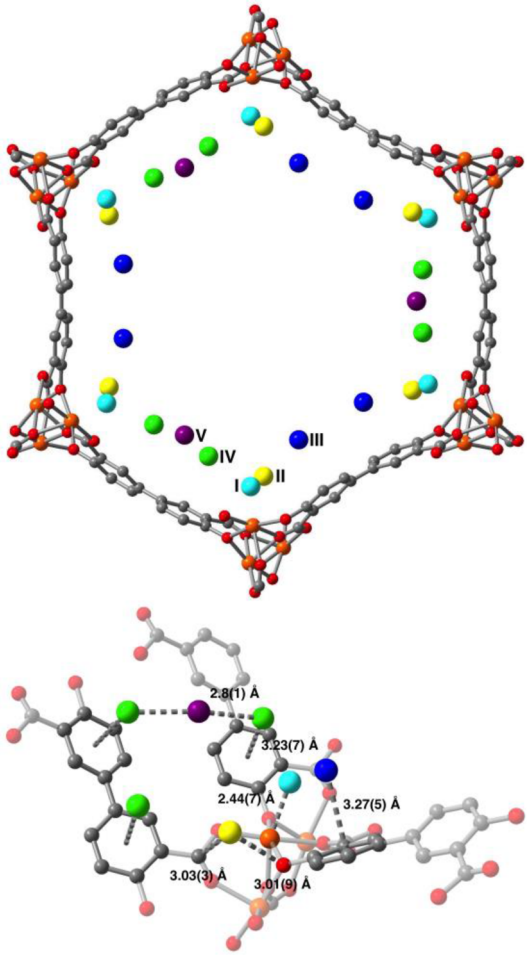

Figure 3. Adsorption sites for D_2 within the structure of Fe_2(dopbdc-d_6), as determined by powder neutron diffraction.

DOI: 10.1021/acs.chemmater.5b04538
Chem. Mater. 2016, 28, 1128−1138

of D_2 per Fe, a single adsorption site, located 2.44(7) Å from the metal, is apparent. As expected based upon the nearly identical coordination geometry and ligand donor environment, the Fe−D_2 distance is within error of the value of 2.47(3) Å observed in Fe_2(dobdc).[72] Upon doubling the D_2 loading to approximately 1.5 per Fe, full occupancy at the first binding site is achieved, along with some population of site II. Similar to site I, binding occurs along the one-dimensional Fe−O chains running the length of the pores approximately halfway between the Fe−D_2 sites with close D_2−carboxylate carbon and D_2−aryloxide oxygen distances of 3.03(3) and 3.01(9) Å, respectively. At 2.75 D_2 molecules per Fe, the saturation of site II is observed, along with some population of two additional binding sites (III and IV) at the faces of the ligand benzene rings. Sites III and IV display similar occupancies of approximately 0.5 with D_2 binding at 3.27(5) Å and 3.23(7) Å, respectively. These values are consistent with previously reported values for analogous D_2−ligand binding. At 4.5 D_2 per Fe, the first four binding sites are fully occupied. Interestingly, it is apparent at this loading that the site IV··· site IV distance of approximately 5.6 Å produces a favorable binding pocket in which an additional D_2 molecule adsorbs. Although these additional binding sites are expected to lead to higher gravimetric H_2 adsorption at high pressure, the increase in empty pore volume is expected to cause M_2(dobpdc) to suffer volumetrically compared to M_2(dobdc).

High-Pressure H_2 Adsorption. To evaluate the hydrogen storage potential of M_2(dobpdc) at ambient temperature, high-pressure adsorption isotherms were collected from 0 to 100 bar at 298 K for all six compounds. At 100 bar, the total gravimetric capacities of the compounds range from 1.3 wt % (M = Zn) to 1.8 wt % (M = Mg) and correlate reasonably well with the respective BET surface areas (Table 1, Figure 4A). Owing to their higher gravimetric surface areas and pore volumes, the M_2(dobpdc) gravimetric capacities are significantly greater than those of M_2(dobdc). For instance, the 100-bar capacity of Co_2(dobpdc) is 1.45 wt %, while that of Co_2(dobdc) is 0.9 wt %. More generally, the total H_2 capacity for a range of metal−organic frameworks at 100 bar and 298 K correlates well the gravimetric BET surface area. This is perhaps not surprising—as surface area increases, the amount of free space inside the framework increases, and there is more bulk H_2 present in empty space that contributes to the total capacity. Because of this, total gravimetric capacity is not the best metric for comparing the H_2 storage performance of different adsorbents. As porosity increases, the mass of framework that occupies a given volume will decrease toward zero, and the total gravimetric capacity will increase toward infinity.

While high-pressure H_2 capacities are routinely reported in the literature in terms of gravimetric uptake, maximizing the volumetric capacity is far more important for H_2 storage applications in passenger vehicles that have limited space for a gas storage system.[90] The volumetric capacity of the M_2(dobpdc) compounds, as calculated using the respective crystallographic densities of the activated frameworks, trends well with the isosteric heats of adsorption and the relative number of accessible strong binding sites. Indeed, Co_2(dobpdc), which has the largest number of accessible strong binding sites, has the highest volumetric uptake at 100 bar and 298 K. As expected, the M_2(dobdc) compounds have higher volumetric capacities than the M_2(dobpdc) compounds, owing to their higher density of strong binding sites.

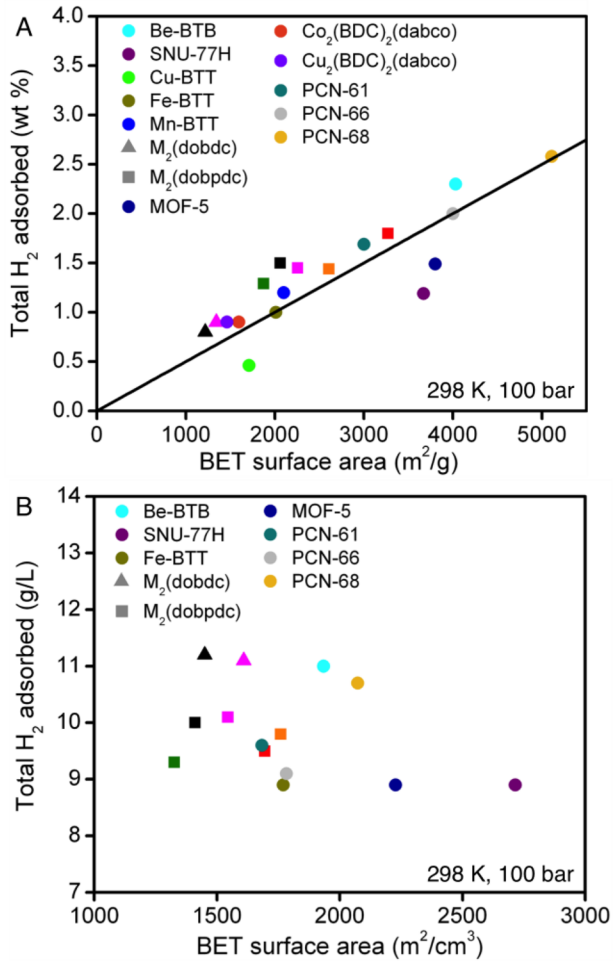

Figure 4. Plots of gravimetric capacity versus gravimetric surface area as well as volumetric capacity versus volumetric surface area for various frameworks.[87−89] Triangles and squares represent the M_2(dobdc) and M_2(dobpdc) framework families respectively with red (Mg), orange (Fe), magenta (Co), black (Ni), and olive (Zn). Additional frameworks are displayed for systematic comparison across a range of gravimetric and volumetric surface areas.

In contrast to the correlation between gravimetric surface area and gravimetric H_2 capacity, volumetric H_2 capacities for M_2(dobpdc) and various other previously reported metal−organic frameworks do not tend to correlate with volumetric surface area (Figure 4B). When considering volumetric uptake, interactions with the framework are most important, and the amount adsorbed is determined primarily by the density and strength of H_2 binding sites rather than simply by the volumetric surface area. As a result, materials that have high surface areas and high total gravimetric capacities but lack any strong binding sites demonstrate much lower volumetric capacities than frameworks with lower surface areas containing strong binding sites.[33,88] For instance, the high density of strong binding sites in Ni_2(dobdc) makes it one of the best materials for on-board H_2 storage, despite its comparatively low volumetric surface area.

CONCLUSIONS AND OUTLOOK

The in-depth and systematic interrogation of hydrogen adsorption in the M_2(dobpdc) series of compounds has shown them to be an excellent platform from which to study high pressure hydrogen storage. Additionally, these frameworks

DOI: 10.1021/acs.chemmater.5b04538
Chem. Mater. 2016, 28, 1128−1138

have illuminated the future directives necessary to achieve efficient on-board hydrogen storage. Past work on metal−organic frameworks for gas storage applications has focused heavily on expanding linker size and achieving large surface areas. However, while gravimetric storage capacity trends linearly upward with surface area, a high volumetric capacity is necessary for efficient fuel storage in transportation applications. Unsurprisingly, this work serves to illustrate how simply expanding a known framework topology, while maintaining isoelectronic and isostructural open metal sites, does not yield an increase in the desired volumetric capacity. Thus, in order to design and develop the next generation of materials for on-board hydrogen storage, it is imperative that the density of open metal sites be maximized. Future work will therefore emphasize the synthesis of new metal−organic-featuring metal centers bearing more than just one open coordination site as a means of increasing the volumetric hydrogen storage capacity.

■ ASSOCIATED CONTENT

Supporting Information

The Supporting Information is available free of charge on the ACS Publications website at DOI: 10.1021/acs.chemmater.5b04538.

77 and 87 K hydrogen adsorption isotherms, linear BET plots, table of performance metrics and physical properties, 77 K H_2 adsorption comparison of Ni_2(dobdc) and Ni_2(dobpdc), atomic parameters from Rietveld refinement of Fe_2(dobpdc), Rietveld refinements of the neutron diffraction patterns of Fe_2(dobpdc), single crystal synthesis and X-ray diffraction, NMR spectra and ESI-MS spectrum for deuteration procedure, ineleastic neutron scattering (PDF)
Crystallographic file for Co_2(dobpdc) (CIF)
Crystallographic file for Fe_2(dobpdc) (CIF)
Crystallographic file for Fe_2(dobpdc)·0.75 D_2(CIF)
Crystallographic file for Fe_2(dobpdc)·1.50 D_2 (CIF)
Crystallographic file for Fe_2(dobpdc)·2.75 D_2 (CIF)
Crystallographic file for Fe_2(dobpdc)·4.50 D_2 (CIF)

■ AUTHOR INFORMATION

Corresponding Author

*E-mail: jrlong@berkeley.edu.

Author Contributions

The manuscript was written through contributions of all authors. All authors have given approval to the final version of the manuscript.

Notes

The authors declare no competing financial interest.

■ ACKNOWLEDGMENTS

Research at Berkeley and NIST was supported through the Department of Energy, Office of Energy Efficiency and Renewable Energy, Fuel Cell Technologies Office. Single crystal X-ray diffraction experiments were performed at beamline 11.3.1 at the Advanced Light Source, a DoE Office of Science User Facility operated by Lawrence Berkeley National Laboratory under Contract No. DE-AC02-05CH11231. Deuteration procedures were performed at the National Deuteration Facility, Australian Nuclear Science and Technology Organisation. Inelastic Neutron Scattering experiments were performed at the ISIS pulsed neutron and muon source at the Rutherford Appleton Laboratory in Oxfordshire, operated by the Science and Technology Facilities Council. We thank Gerald K. Branch and Arkema for fellowship support of E.D.B., the NIST/NRC Fellowship program for support of M.R.H., the National Science Foundation for fellowship support of J.A.M. Portions of this work were performed at the Molecular Foundry, supported by the U.S. Department of Energy, Office of Science, Office of Basic Energy Sciences.

■ REFERENCES

(1) Ogden, J. M.; Steinbugler, M. M.; Kreutz, T. G. A comparison of hydrogen, methanol and gasoline as fuels for fuel cell vehicles: implications for vehicle design and infrastructure development. *J. Power Sources* **1999**, *79*, 143−168.
(2) Kamat, P. V.; Bisquert, J. Solar Fuels. Photocatalytic Hydrogen Generation. *J. Phys. Chem. C* **2013**, *117*, 14873−14875.
(3) Alternative Fuels Data Center. www.afdc.energy.gov/fuels/hydrogen.html (accessed August 26, 2013).
(4) EERE: Hydrogen, Fuel Cells, & Infrastructure Technologies Program Storage Targets. http://www1.eere.energy.gov/hydrogenandfuelcells/storage/pdfs/targetsonboardhydrostorage.pdf (accessed August 2012).
(5) Sakintuna, B.; Lamari-Darkrim, F.; Hirscher, M. Metal hydride materials for solid hydrogen storage: A review. *Int. J. Hydrogen Energy* **2007**, *32*, 1121−1140.
(6) Schlapbach, L.; Züttel, A. Hydrogen Storage Materials for Mobile Applications. *Nature* **2001**, *414*, 353−358.
(7) Zuettel, A. Materials for hydrogen storage. *Mater. Today* **2003**, *6*, 24−33.
(8) Weitkamp, J.; Fritz, M.; Ernst, S. Zeolites as media for hydrogen storage. *Int. J. Hydrogen Energy* **1995**, *20*, 967−970.
(9) Yang, Z.; Xia, Y.; Mokaya, R. Enhanced Hydrogen Storage Capacity of High Surface Area Zeolite-like Carbon Materials. *J. Am. Chem. Soc.* **2007**, *129*, 1673−1679.
(10) Ricchiardi, G.; Vitillo, J. G.; Cocina, D.; Gribov, E. N.; Zecchina, A. Direct observation and modelling of ordered hydrogen adsorption and catalyzed ortho−para conversion on ETS-10 titanosilicate material. *Phys. Chem. Chem. Phys.* **2007**, *9*, 2753−2760.
(11) Bhatia, S. K.; Myers, A. L. Optimum Conditions for Adsorptive Storage. *Langmuir* **2006**, *22*, 1688−1700.
(12) Rowsell, J. L. C.; Millward, A. R.; Park, K. S.; Yaghi, O. M. Hydrogen Sorption in Functionalized Metal−Organic Frameworks. *J. Am. Chem. Soc.* **2004**, *126*, 5666−5667.
(13) Rowsell, J. L. C.; Yaghi, O. M. Strategies for Hydrogen Storage in Metal−Organic Frameworks. *Angew. Chem., Int. Ed.* **2005**, *44*, 4670−4679.
(14) Millward, A. R.; Yaghi, O. M. Metal−Organic Frameworks with Exceptionally High Capacity for Storage of Carbon Dioxide at Room Temperature. *J. Am. Chem. Soc.* **2005**, *127*, 17998−17999.
(15) Wong-Foy, A. G.; Matzger, A. J.; Yaghi, O. M. Exceptional H_2 Saturation Uptake in Microporous Metal−Organic Frameworks. *J. Am. Chem. Soc.* **2006**, *128*, 3494−3495.
(16) Wu, H.; Zhou, W.; Yildirim, T. Hydrogen Storage in a Prototypical Zeolitic Imidazolate Framework-8. *J. Am. Chem. Soc.* **2007**, *129*, 5314−5315.
(17) Kaye, S. S.; Dailly, A.; Yaghi, O. M.; Long, J. R. Impact of Preparation and Handling on the Hydrogen Storage Properties of Zn_4O(1,4-benzenedicarboxylate)$_3$ (MOF-5). *J. Am. Chem. Soc.* **2007**, *129*, 14176−14177.
(18) Li, Y.; Yang, R. T. Gas Adsorption and Storage in Metal−Organic Framework MOF-177. *Langmuir* **2007**, *23*, 12937−12944.
(19) Dincă, M.; Long, J. R. Hydrogen Storage in Microporous Metal−Organic Frameworks with Exposed Metal Sites. *Angew. Chem., Int. Ed.* **2008**, *47*, 6766−6779.
(20) Murray, L. J.; Dincă, M.; Long, J. R. Hydrogen storage in metal−organic frameworks. *Chem. Soc. Rev.* **2009**, *38*, 1294−1314.
(21) Getman, R. B.; Bae, Y.; Wilmer, C. E.; Snurr, R. Q. Review and Analysis of Molecular Simulations of Methane, Hydrogen, and

DOI: 10.1021/acs.chemmater.5b04538
Chem. Mater. 2016, 28, 1128−1138

Acetylene Storage in Metal−Organic Frameworks. *Chem. Rev.* **2012**, *112*, 703−723.
(22) Suh, M. P.; Park, H. J.; Prasad, T. K.; Lim, D.-W. Hydrogen Storage in Metal−Organic Frameworks. *Chem. Rev.* **2012**, *112*, 782−835.
(23) Sumida, K.; Hill, M. R.; Horike, S.; Dailly, A.; Long, J. R. Synthesis and Hydrogen Storage Properties of $Be_{12}(OH)_{12}$(1,3,5-benzenetribenzoate)$_4$. *J. Am. Chem. Soc.* **2009**, *131*, 15120−15121.
(24) Bae, Y.-S.; Dubbeldam, D.; Nelson, A.; Walton, K. S.; Hupp, J. T.; Snurr, R. Q. Strategies for Characterization of Large-Pore Metal-Organic Frameworks by Combined Experimental and Computational Methods. *Chem. Mater.* **2009**, *21*, 4768−4777.
(25) Martin, R. M.; Haranczyk, M. Exploring frontiers of high surface area metal−organic frameworks. *Chem. Sci.* **2013**, *4*, 1781−1785.
(26) Chae, H. K.; Siberio-Pérez, D. Y.; Kim, J.; Go, Y.; Eddaoudi, M.; Matzger, A. J.; O'Keeffe, M.; Yaghi, O. M. A route to high surface area, porosity and inclusion of large molecules in crystals. *Nature* **2004**, *427*, 523−527.
(27) Farha, O. K.; Eryazici, I.; Jeong, N. C.; Hauser, B. G.; Wilmer, C. E.; Sarjeant, A. A.; Snurr, R. Q.; Nguyen, S. T.; Yazaydin, A. Ö.; Hupp, J. T. Metal−Organic Framework Materials with Ultrahigh Surface Areas: Is the Sky the Limit? *J. Am. Chem. Soc.* **2012**, *134*, 15016−15021.
(28) Dincă, M.; Dailly, A.; Liu, Y.; Brown, C. M.; Neumann, D. A.; Long, J. R. Hydrogen Storage in a Microporous Metal−Organic Framework with Exposed Mn^{2+} Coordination Sites. *J. Am. Chem. Soc.* **2006**, *128*, 16876−16883.
(29) Dincă, M.; Long, J. R. High-Enthalpy Hydrogen Adsorption in Cation-Exchanged Variants of the Microporous Metal−Organic Framework $Mn_3[(Mn_4Cl)_3(BTT)_8(CH_3OH)_{10}]_2$. *J. Am. Chem. Soc.* **2007**, *129*, 11172−11176.
(30) Dincă, M.; Han, W. S.; Liu, Y.; Dailly, A.; Brown, C. M.; Long, J. R. Observation of Cu^{2+}−H_2 Interactions in a Fully Desolvated Sodalite-Type Metal−Organic Framework. *Angew. Chem., Int. Ed.* **2007**, *46*, 1419−1422.
(31) Ouellette, W.; Darling, K.; Prosvirin, A.; Whitenack, K.; Dunbar, K. R.; Zubieta, J. Syntheses, structural characterization and properties of transition metal complexes of 5,5′-(1,4-phenylene)bis(1*H*-tetrazole) (H_2bdt), 5′,5″-(1,1′-biphenyl)-4,4′-diylbis(1*H*-tetrazole) (H_2dbdt) and 5,5′,5″-(1,3,5-phenylene)tris(1*H*-tetrazole) (H_3btt). *Dalton Trans.* **2011**, *40*, 12288−12300.
(32) Sumida, K.; Stück, D.; Mino, L.; Chai, J.-D.; Bloch, E. D.; Zavorotynska, O.; Murray, L. J.; Dincă, M.; Chavan, S.; Bordiga, S.; Head-Gordon, M.; Long, J. R. Impact of Metal and Anion Substitutions on the Hydrogen Storage Properties of M-BTT Metal−Organic Frameworks. *J. Am. Chem. Soc.* **2013**, *135*, 1083−1091.
(33) Sumida, K.; Horike, S.; Kaye, S. S.; Herm, Z. R.; Queen, W. L.; Brown, C. M.; Grandjean, F.; Long, G. J.; Long, J. R.; Dailly, A. Hydrogen storage and carbon dioxide capture in an iron-based sodalite-type metal−organic framework (Fe-BTT) discovered via high-throughput methods. *Chem. Sci.* **2010**, *1*, 184−191.
(34) Rosi, N. L.; Kim, J.; Eddaoudi, M.; Chen, B.; O'Keeffe, M.; Yaghi, O. M. Rod Packings and Metal−Organic Frameworks Constructed from Rod-Shaped Secondary Building Units. *J. Am. Chem. Soc.* **2005**, *127*, 1504−1518.
(35) Dietzel, P. D. C.; Morita, Y.; Blom, R.; Fjellvåg, H. An In Situ High-Temperature Single-Crystal Investigation of a Dehydrated Metal−Organic Framework Compound and Field-Induced Magnetization of One-Dimensional Metal−Oxygen Chains. *Angew. Chem., Int. Ed.* **2005**, *44*, 6354−6358.
(36) Dietzel, P. D. C.; Panella, B.; Hirscher, M.; Blom, R.; Fjellvåg, H. Hydrogen adsorption in a nickel based coordination polymer with open metal sites in the cylindrical cavities of the desolvated framework. *Chem. Commun.* **2006**, 959−961.
(37) Dietzel, P. D. C.; Blom, R.; Fjellvåg, H. Base-Induced Formation of Two Magnesium Metal-Organic Framework Compounds with a Bifunctional Tetratopic Ligand. *Eur. J. Inorg. Chem.* **2008**, 3624−3632.
(38) Zhou, W.; Wu, H.; Yildirim, T. Enhanced H_2 Adsorption in Isostructural Metal−Organic Frameworks with Open Metal Sites: Strong Dependence of the Binding Strength on Metal Ions. *J. Am. Chem. Soc.* **2008**, *130*, 15268−15269.
(39) Bloch, E. D.; Murray, L. J.; Queen, W. L.; Chavan, S.; Maximoff, S. N.; Bigi, J. P.; Krishna, R.; Peterson, V. K.; Grandjean, F.; Long, G. J.; Smit, B.; Bordiga, S.; Brown, C. M.; Long, J. R. Selective Binding of O_2 over N_2 in a Redox−Active Metal−Organic Framework with Open Iron(II) Coordination Sites. *J. Am. Chem. Soc.* **2011**, *133*, 14814−14822.
(40) Sanz, R.; Martínez, F.; Orcajo, G.; Wojtas, L.; Briones, D. Synthesis of a honeycomb-like Cu-based metal−organic framework and its carbon dioxide adsorption behavior. *Dalton Trans.* **2013**, *42*, 2392−2398.
(41) Díaz-García, M.; Sánchez-Sánchez, M. Synthesis and characterization of a new Cd-based metal-organic framework isostructural with MOF-74/CPO-27 materials. *Microporous Mesoporous Mater.* **2014**, *190*, 248−254.
(42) Sumida, K.; Her, J.-H.; Dincă, M.; Murray, L. J.; Schloss, J. M.; Pierce, C. J.; Thompson, B. A.; Fitzgerald, S. A.; Brown, C. M.; Long, J. R. Neutron Scattering and Spectroscopic Studies of Hydrogen Adsorption in $Cr_3(BTC)_2$—A Metal−Organic Framework with Exposed Cr^{2+} Sites. *J. Phys. Chem. C* **2011**, *115*, 8414−8421.
(43) Wade, C. R.; Dincă, M. Investigation of the synthesis, activation, and isosteric heats of CO_2 adsorption of the isostructural series of metal−organic frameworks $M_3(BTC)_2$ (M = Cr, Fe, Ni, Cu, Mo, Ru). *Dalton. Trans.* **2012**, *41*, 7931−7938.
(44) Brozek, C. K.; Dincă, M. Lattice-imposed geometry in metal−organic frameworks: lacunary Zn_4O clusters in MOF-5 serve as tripodal chelating ligands for Ni^{2+}. *Chem. Sci.* **2012**, *3*, 2110−2113.
(45) Brozek, C. K.; Dincă, M. Ti^{3+}-, $V^{2+/3+}$-, $Cr^{2+/3+}$-, Mn^{2+}-, and Fe^{2+}-Substituted MOF-5 and Redox Reactivity in Cr- and Fe-MOF-5. *J. Am. Chem. Soc.* **2013**, *135*, 12886−12981.
(46) Brozek, C. K.; Dincă, M. Thermodynamic parameters of cation exchange in MOF-5 and MFU-41. *Chem. Commun.* **2015**, *51*, 11780−11782.
(47) Wiers, B. M.; Foo, M.-L.; Balsara, N.; Long, J. R. A Solid Lithium Electrolyte via Addition of Lithium Isopropoxide to a Metal−Organic Framework with Open Metal Sites. *J. Am. Chem. Soc.* **2011**, *133*, 14522−14525.
(48) Kobayashi, Y.; Jacobs, B.; Allendorf, M. D.; Long, J. R. Conductivity, Doping, and Redox Chemistry of a Microporous Dithiolene-Based Metal−Organic Framework. *Chem. Mater.* **2010**, *22*, 4120−4122.
(49) Aubrey, M. L.; Ameloot, R.; Wiers, B. M.; Long, J. R. Metal−organic frameworks as solid magnesium electrolytes. *Energy Environ. Sci.* **2014**, *7*, 667−671.
(50) Talin, A. A.; Centrone, A.; Ford, A. C.; Foster, M. E.; Stavila, V.; Haney, P.; Kinney, A.; Szalai, V.; El Gabaly, F.; Yoon, H. P.; Léonard, F.; Allendorf, M. D. Tunable Electrical Conductivity in Metal-Organic Framework Thin-Film Devices. *Science* **2014**, *343*, 66−69.
(51) Horcajada, P.; Serre, C.; Maurin, G.; Ramsahye, N. A.; Balas, F.; Vallet-Regí, M.; Sebban, M.; Taulelle, F.; Férey, G. Flexible Porous Metal-Organic Frameworks for a Controlled Drug Delivery. *J. Am. Chem. Soc.* **2008**, *130*, 6774−6780.
(52) Bloch, E. D.; Queen, W. L.; Chavan, S.; Wheatley, P. S.; Zadrozny, J. M.; Morris, R.; Brown, C. M.; Lamberti, C.; Bordiga, S.; Long, J. R. Gradual Release of Strongly Bound Nitric Oxide from $Fe_2(NO)_2$(dobdc). *J. Am. Chem. Soc.* **2015**, *137*, 3466−3469.
(53) Xiao, D. J.; Bloch, E. D.; Mason, J. A.; Queen, W. L.; Hudson, M. R.; Planas, N.; Borycz, J.; Dzubak, A. L.; Verma, P.; Lee, K.; Bonino, F.; Crocellà, V.; Yano, J.; Bordiga, S.; Truhlar, D. G.; Gagliardi, L.; Brown, C. M.; Long, J. R. Oxidation of ethane to ethanol by N_2O in a metal−organic framework with coordinatively unsaturated iron(II) sites. *Nat. Chem.* **2014**, *6*, 590−595.
(54) Gonzalez, M. I.; Bloch, E. D.; Mason, J. A.; Teat, S. J.; Long, J. R. Single-Crystal-to-Single-Crystal Metalation of a Metal−Organic Framework: A Route toward Structurally Well-Defined Catalysts. *Inorg. Chem.* **2015**, *54*, 2995−3005.

DOI: 10.1021/acs.chemmater.5b04538
Chem. Mater. 2016, 28, 1128−1138

(55) Mlinar, A. N.; Keitz, B. K.; Gygi, D.; Bloch, E. D.; Long, J. R.; Bell, A. T. Selective Propene Oligomerization with Nickel(II)-Based Metal−Organic Frameworks. *ACS Catal.* **2014**, *4*, 717−721.
(56) Liu, Y.; Kabbour, H.; Brown, C. M.; Neumann, D. A.; Ahn, C. C. Increasing the Density of Adsorbed Hydrogen with Coordinatively Unsaturated Metal Centers in Metal−Organic Frameworks. *Langmuir* **2008**, *24*, 4772−4777.
(57) Dietzel, P. D. C.; Johnsen, R. E.; Fjellvag, H.; Bordiga, S.; Groppo, E.; Chavan, S.; Blom, R. Adsorption properties and structure of CO_2 adsorbed on open coordination sites of metal−organic framework Ni_2(dhtp) from gas adsorption, IR spectroscopy and X-ray diffraction. *Chem. Commun.* **2008**, 5125−5127.
(58) Britt, D.; Furukawa, H.; Wang, B.; Glover, T. G.; Yaghi, O. M. Highly efficient separation of carbon dioxide by a metal-organic framework replete with open metal sites. *Proc. Natl. Acad. Sci. U. S. A.* **2009**, *106*, 20637−20640.
(59) Dietzel, P. D. C.; Besikiotis, V.; Blom, R. Application of metal−organic frameworks with coordinatively unsaturated metal sites in storage and separation of methane and carbon dioxide. *J. Mater. Chem.* **2009**, *19*, 7362−7370.
(60) Herm, Z. R.; Swisher, J. A.; Smit, B.; Krishna, R.; Long, J. R. Metal−Organic Frameworks as Adsorbents for Hydrogen Purification and Precombustion Carbon Dioxide Capture. *J. Am. Chem. Soc.* **2011**, *133*, 5664−5667.
(61) Mason, J. A.; Sumida, K.; Herm, Z. R.; Krishna, R.; Long, J. R. Evaluating metal−organic frameworks for post-combustion carbon dioxide capture via temperature swing adsorption. *Energy Environ. Sci.* **2011**, *4*, 3030−3040.
(62) Bloch, E. D.; Queen, W. L.; Krishna, R.; Zadrozny, J. M.; Brown, C. M.; Long, J. R. Hydrocarbon Separations in a Metal-Organic Framework with Open Iron(II) Coordination Sites. *Science* **2012**, *335*, 1606−1610.
(63) Kong, X.; Scott, E.; Ding, W.; Mason, J. A.; Long, J. R.; Reimer, J. A. CO_2 Dynamics in a Metal−Organic Framework with Open Metal Sites. *J. Am. Chem. Soc.* **2012**, *134*, 14341−14344.
(64) Geier, S. J.; Mason, J. A.; Bloch, E. D.; Queen, W. L.; Hudson, M. R.; Brown, C. M.; Long, J. R. Selective adsorption of ethylene over ethane and propylene over propane in the metal−organic frameworks M_2(dobdc) (M = Mg, Mn, Fe, Co, Ni, Zn). *Chem. Sci.* **2013**, *4*, 2054−2061.
(65) Herm, Z. R.; Krishna, R.; Long, J. R. CO_2/CH_4, CH_4/H_2 and $CO_2/CH_4/H_2$ separations at high pressures using Mg_2(dobdc). *Microporous Mesoporous Mater.* **2012**, *151*, 481−487.
(66) Yu, D.; Yazaydin, O.; Lane, J. R.; Dietzel, P. D. C.; Snurr, R. Q. A combined experimental and quantum chemical study of CO_2 adsorption in the metal−organic framework CPO-27 with different metals. *Chem. Sci.* **2013**, *4*, 3544−3556.
(67) Lee, K.; Isley, W. C., III; Dzubak, A. L.; Verma, P.; Stoneburner, S. J.; Lin, L. C.; Howe, J. D.; Bloch, E. D.; Reed, D. A.; Hudson, M. R.; Brown, C. M.; Long, J. R.; Neaton, J. B.; Smit, B.; Cramer, C. J.; Truhlar, D. G.; Gagliardi, L. Design of a Metal−Organic Framework with Enhanced Back Bonding for Separation of N_2 and CH_4. *J. Am. Chem. Soc.* **2014**, *136*, 698−704.
(68) Herm, Z. R.; Bloch, E. D.; Long, J. R. Hydrocarbon Separations in Metal−Organic Frameworks. *Chem. Mater.* **2014**, *26*, 323−338.
(69) Wu, H.; Simmons, J. M.; Srinivas, G.; Zhou, W.; Yildirim, T. Adsorption Sites and Binding Nature of CO_2 in Prototypical Metal−Organic Frameworks: A Combined Neutron Diffraction and First-Principles Study. *J. Phys. Chem. Lett.* **2010**, *1*, 1946−1951.
(70) Sumida, K.; Brown, C. M.; Herm, Z. R.; Chavan, S.; Bordiga, S.; Long, J. R. Hydrogen storage properties and neutron scattering studies of Mg_2(dobdc)—a metal−organic framework with open Mg^{2+} adsorption sites. *Chem. Commun.* **2011**, *47*, 1157−1159.
(71) Queen, W. L.; Brown, C. M.; Britt, D. K.; Zajdel, P.; Hudson, M. R.; Yaghi, O. M. Site-Specific CO_2 Adsorption and Zero Thermal Expansion in an Anisotropic Pore Network. *J. Phys. Chem. C* **2011**, *115*, 24915−24919.
(72) Queen, W. L.; Bloch, E. D.; Brown, C. M.; Hudson, M. R.; Mason, J. A.; Murray, L. J.; Ramirez-Cuesta, A. J.; Peterson, V. K.; Long, J. R. Hydrogen adsorption in the metal−organic frameworks Fe_2(dobdc) and $Fe_2(O_2)$ (dobdc). *Dalton Trans.* **2012**, *41*, 4180−4187.
(73) Brown, C. M.; Ramirez-Cuesta, A. J.; Her, J.-H.; Wheatley, P. S.; Morris, R. E. Structure and spectroscopy of hydrogen adsorbed in a nickel metal−organic framework. *Chem. Phys.* **2013**, *427*, 3−8.
(74) Kapelewski, M. T.; Geier, S. J.; Hudson, M. R.; Stück, D.; Mason, J. A.; Nelson, J. N.; Xiao, D. J.; Hulvey, Z.; Gilmour, E.; FitzGerald, S. A.; Head-Gordon, M.; Brown, C. M.; Long, J. R. M_2(*m*-dobdc) (M = Mg, Mn, Fe, Co, Ni) Metal−Organic Frameworks Exhibiting Increased Charge Density and Enhanced H_2 Binding at the Open Metal Sites. *J. Am. Chem. Soc.* **2014**, *136*, 12119−12129.
(75) Deng, H.; Grunder, S.; Cordova, K. E.; Valente, C.; Furukawa, H.; Hmadeh, M.; Gandara, F.; Whalley, A. C.; Liu, Z.; Asahina, S.; Kazumori, H.; O'Keeffe, M.; Terasaki, O.; Stoddart, J. F.; Yaghi, O. M. Large-Pore Apertures in a Series of Metal-Organic Frameworks. *Science* **2012**, *336*, 1018−1023.
(76) McDonald, T. M.; Lee, W. R.; Mason, J. A.; Wiers, B. M.; Hong, C. S.; Long, J. R. Capture of Carbon Dioxide from Air and Flue Gas in the Alkylamine-Appended Metal−Organic Framework mmen-Mg_2(dobpdc). *J. Am. Chem. Soc.* **2012**, *134*, 7056−7065.
(77) Lin, L. C.; Kim, J.; Kong, X.; Scott, E.; McDonald, T. M.; Long, J. R.; Reimer, J. A.; Smit, B. Understanding CO_2 Dynamics in Metal−Organic Frameworks with Open Metal Sites. *Angew. Chem., Int. Ed.* **2013**, *52*, 4410−4413.
(78) McDonald, T. M.; Mason, J. A.; Kong, X.; Bloch, E. D.; Gygi, D.; Dani, A.; Crocella, V.; Giordanino, F.; Odoh, S. O.; Drisdell, W. S.; Vlaisavljevich, B.; Dzubak, A. L.; Poloni, R.; Schnell, S. K.; Planas, N.; Lee, K.; Pascal, T.; Wan, L. F.; Prendergast, D.; Neaton, J. B.; Smit, B.; Kortright, J. B.; Gagliardi, L.; Bordiga, S.; Reimer, J. A.; Long, J. R. Cooperative insertion of CO_2 in diamine-appended metal-organic frameworks. *Nature* **2015**, *519*, 303−308.
(79) Toby, B. H. EXPGUI, a graphical user interface for GSAS. *J. Appl. Crystallogr.* **2001**, *34*, 210−213.
(80) Larson, A. C.; Von Dreele, R. B. *General Structure Analysis System (GSAS)*; Los Alamos National Laboratory Report LAUR: Los Alamos, New Mexico, 1994; pp 86−748.
(81) Walton, K. S.; Snurr, R. Q. Applicability of the BET Method for Determining Surface Areas of Microporous Metal−Organic Frameworks. *J. Am. Chem. Soc.* **2007**, *129*, 8552−8556.
(82) Queen, W. L.; Hudson, M. R.; Bloch, E. D.; Mason, J. A.; Gonzalez, M. I.; Lee, J. S.; Gygi, D.; Howe, J. D.; Lee, K.; Darwish, T.; James, M.; Peterson, V. K.; Teat, S. J.; Smit, B.; Neaton, J. B.; Long, J. R.; Brown, C. M. Comprehensive study of carbon dioxide adsorption in the metal−organic frameworks M_2(dobdc) (M = Mg, Mn, Fe, Co, Ni, Cu, Zn). *Chem. Sci.* **2014**, *5*, 4569−4581.
(83) Vitillo, J. G.; Regli, L.; Chavan, S.; Ricchiardi, G.; Spoto, G.; Dietzel, P. D. C.; Bordiga, S.; Zecchina, A. Role of Exposed Metal Sites in Hydrogen Storage in MOFs. *J. Am. Chem. Soc.* **2008**, *130*, 8386−8396.
(84) Rowsell, J. L. C.; Yaghi, O. M. Effects of Functionalization, Catenation, and Variation of the Metal Oxide and Organic Linking Units on the Low-Pressure Hydrogen Adsorption Properties of Metal−Organic Frameworks. *J. Am. Chem. Soc.* **2006**, *128*, 1304−1315.
(85) Irving, H.; Williams, J. P. Order of Stability of Metal Complexes. *Nature* **1948**, *162*, 746−747.
(86) Sato, H.; Kosaka, W.; Matsuda, R.; Hori, A.; Hijikata, Y.; Belosludov, R. V.; Sakaki, S.; Takata, M.; Kitagawa, S. Self-Accelerating CO Sorption in a Soft Nanoporous Crystal. *Science* **2014**, *343*, 167−170.
(87) Takei, T.; Kawashima, J.; Ii, T.; Maeda, A.; Hasegawa, M.; Kitagawa, T.; Ohmura, T.; Ichikawa, M.; Hosoe, M.; Kanoya, I.; Mori, W. Hydrogen Adsorption Properties of Lantern-Type Dinuclear M(BDC) $(DABCO)_{1/2}$. *Bull. Chem. Soc. Jpn.* **2008**, *81*, 847−856.
(88) Yuan, D.; Zhao, D.; Sun, D.; Zhou, H.-C. An Isoreticular Series of Metal−Organic Frameworks with Dendritic Hexacarboxylate Ligands and Exceptionally High Gas-Uptake Capacity. *Angew. Chem., Int. Ed.* **2010**, *49*, 5357−5361.

DOI: 10.1021/acs.chemmater.5b04538
Chem. Mater. 2016, 28, 1128−1138

(89) Park, H. J.; Lim, D.-W.; Yang, W. S.; Oh, T.-R.; Suh, M. P. A Highly Porous Metal−Organic Framework: Structural Transformations of a Guest-Free MOF Depending on Activation Method and Temperature. *Chem. Eur. J.* **2011**, *17*, 7251−7260.
(90) Mason, J. A.; Veenstra, M.; Long, J. R. Evaluating metal−organic frameworks for natural gas storage. *Chem. Sci.* **2014**, *5*, 32−51.

DOI: 10.1021/acs.chemmater.5b04538
Chem. Mater. 2016, 28, 1128−1138